Solid Oxide Fuel Cell Performance Studies

Wayne Huebner (huebner@umr.edu; 573-341-6129)
David M. Reed (dreed@umr.edu; 573-341-6125)
Harlan U. Anderson (harlanua@umr.edu; 573-341-4886)

Department of Ceramic Engineering
University of Missouri - Rolla
222 McNutt Hall
Rolla, MO 65401

1.0 INTRODUCTION

Materials research in the area of SOFC's is also driven by the recognition that processing and operating at lower temperatures would circumvent most of the reliability problems which are currently preventing these devices from achieving wide-scale commercialization. These considerations have directed interdisciplinary research thrusts in this field, namely:

- Alternate Materials
  - → higher conductivities at lower temperatures for all four SOFC components
  - → mixed-conducting cathodes
  - → greater phase stability at low pO_2's
- Processing
  - → novel synthesis techniques (for powders and thin films)
  - → controlled microstructure with desired properties
- Reliability Issues
  - → chemical, mechanical, and electrical stability under the temperature/time/atmosphere conditions of cofiring and operation

Hence studies on the optimization of components use of mixed conductors and thin film processing techniques, as well as studies on structure↔property relationships represent an enabling technology; what remains is to utilize this technology for the fabrication of planar SOFC's. In this portion of the research we are focusing on the microstructure ↔ property relations in solid oxide fuel cells (SOFC's) to better understand the mechanisms involved in cell performance. The aim is to fabricate SOFC's with controlled microstructures utilizing $La_{1-x}Sr_xMnO_3$ (LSM), yttria stabilized zirconia (YSZ), and Ni-YSZ composites as the cathode, electrolyte, and anode, respectively. Ideally, the electrode materials would be tailored for an increased reaction rate (grain size ≤ 1 μm), be stable with time (> 10,000 h), have a thermal expansion match to YSZ (α~11 x 10^{-6}/°C), show limited chemical interaction with the electrolyte, and show no degradation in electrical performance. This paper describes starting powder characteristics, electrical conductivity and overpotential measurements, and resultant microstructures as a function of processing conditions (i.e. powder calcination temperature, and annealing temperature) and composition for the electrolyte and cathodes.

2.0 OBJECTIVES

The University of Missouri-Rolla is performing a 5 year research program with two primary objectives: 1) developing $LaCrO_3$-based interconnect powders which densify when in contact with anode and cathode materials for solid oxide fuel cells (SOFC), and 2) developing high performance cathodes, anodes and interfaces for use in planar SOFC's. The latter is the focus of this paper. With regard to developing high performance materials for use in planar SOFC's, the specific objectives of this research program over the last year have been to:

- Fabricate single cells with controlled microstructures (i.e. grain size and porosity of electrodes) for operation at 1000°C.
- Gain a better understanding of the mechanisms involved in improving cell performance via electrochemical and impedance techniques.
- Develop processing ↔ microstructure ↔ property relations of electrodes and their corresponding interfacial reactions.

3.0 Experimental Procedure

3.1 Apparatus Construction

The system constructed for measuring cell performance is a Kanthal-heated, three-zone, half-shell furnace (1100°C) mounted such that samples can be loaded from either top or bottom. Each zone is three inches in diameter and length and is controlled a by Love Model 1600 temperature controller. The self supporting electrolyte was mounted and sealed to two mullite tubes ~28 mm OD and ~22 mm ID as shown in Figure 1. A mullite tube with an inner diameter slightly larger than 28 mm (~29mm) was cut into ~7 mm thick washers and super glued onto each side of the electrolyte. A ceramic adhesive/sealant, Aremco 503, was then applied at the electrolyte/mullite washer interfaces. The sealant is an alumina-based cement with working temperatures up to 1650°C. The mullite washers acted as collars and helped to align the samples and improve the sealing quality. The mullite tubes used for atmosphere control were then place inside the mullite washers and sealed to the electrolyte. The samples were heated at ~ 2°C/min and held at 1000°C until all characterization was completed. Samples could not be thermally cycled due to the difference in thermal expansion, 7.5 and 10.5 ppm/°C for the cement and YSZ electrolyte, respectively. Upon cooling to room temperature the mullite washers and tubes remained bonded to one another whereas the YSZ sample could be easily detached.

Both mullite tubes were sealed to the ends of a silica tube of 63.5 mm (2 1/2") OD by use of aluminum faceplates, silicone O-rings, and a Vacoa seal (Figure 2). Gas inlet and outlet ports were drilled into the aluminum faceplates and sealed using Swagelock connectors. The outer end of the mullite tubes were also sealed using stainless steel faceplates and silicone O-rings. Pt and Ni wires for cathode and anode sensing, respectively, were inserted into the alumina tubes to make electrical connection to the YSZ electrolyte. Baffles made of sali board were placed inside the mullite tubes

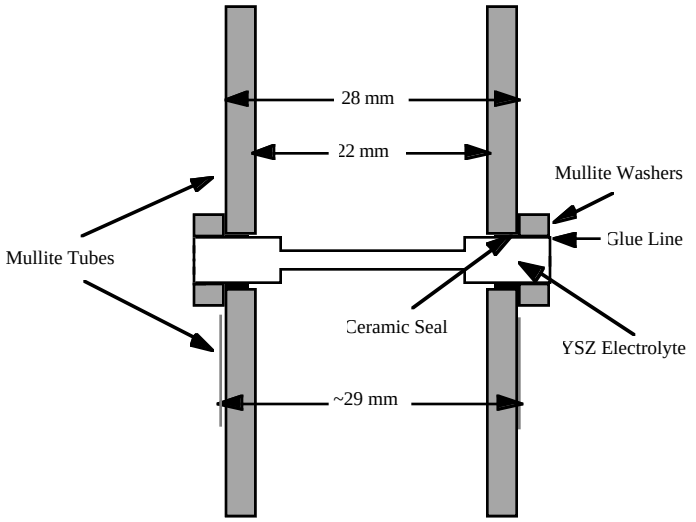

Figure 1. Schematic illustration of the method used for mounting self-supporting YSZ electrolytes.

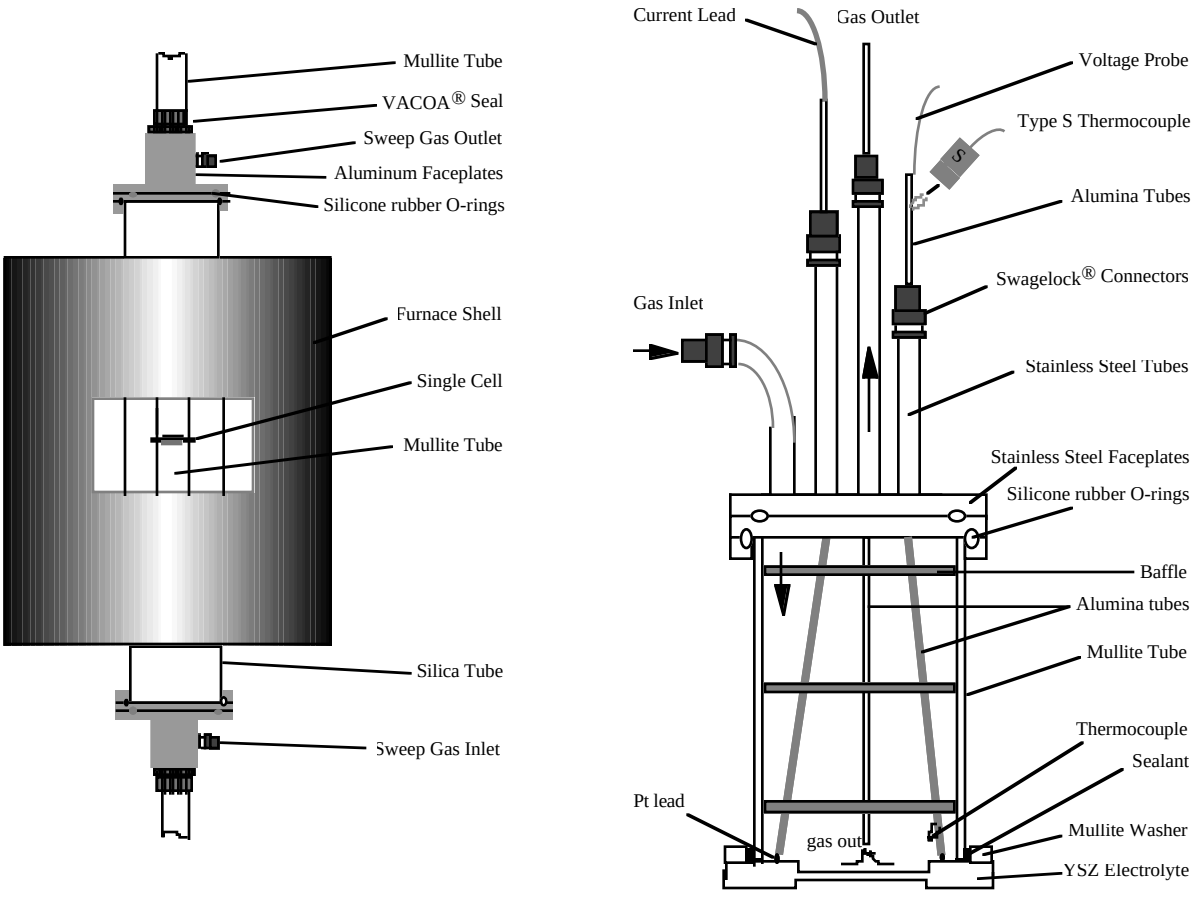

Figure 2. Schematic illustrations of the SOFC measurement system.

to help mixing of the gases and also acted as positioners for the alumina thermocouple tubes to ensure proper electrical connection.

Both oxidant and fuel flow rates were controlled to the sample via the mullite tubes using Tylan Model FC-260 mass flow controllers. Air was used as the oxidant in the majority of experiments, with a flow rate of 200 sccm. Pure oxygen was also used in some experiments and was delivered at a rate of 200 sccm. A mixture of forming gas, FG, (90% N_2 - 10% H_2) and CO_2 was used as the fuel and had corresponding flow rates of 200 and 2 sccm, respectively. The FG-CO_2 mixture gave Nernst potentials of 1.00 and 1.05 V with air and O_2, respectively. The FG-CO_2 mixture had a pO_2 equal to $10^{-16.5}$ at 1000°C. Nitrogen was delivered into the silica to sweep away any oxidant or fuel leaking out of the active region of the cell. In all experiments air was introduced in the top tube, fuel to the bottom tube, and the sweep gas was fed to the bottom and exited the top.

Outlet gases were monitored with Porter ball flow meters to determine if the sample was sealed, and also if the electrolyte had fractured. A greater pressure was created in the oxidant and fuel gases compared to the sweep gas by bubbling the exhaust gas, oxidant and fuel, in oil. This ensured that if a leak occurred at the seal that the oxidant and fuel would leak into the silica tube and mix with the sweep gas rather than vice versa.

3.2 Materials Selection, Preparation and Characterization

The purpose of this investigation was to study the influence of microstructure and composition on the performance of single SOFCs. Commercially available Y stabilized ZrO_2 (YSZ) powders were used in this study for the electrolyte and as a major constituent in the anode. Cathode, $La_xSr_{0.2}MnO_3$ ($0.7 \leq x \leq 0.79$) and anode [YSZ-$Ni_{1-x}Mg_xO$ ($x = 0.0, 0.1$)], compositions were synthesized by the liquid mix and the glycine nitrate methods, respectively. In this paper only results associated with the cathode will be presented.

Yttria stabilized ZrO_2

The commercially available Y doped ZrO_2 (Zirconia Sales of America Inc.) is a fully stabilized (8 mole % Y_2O_3), co-precipitated powder. This particular powder was chosen because of its low cost, ~$70/kg, low impurity content and low densification temperature, ~1400°C. The YSZ powder had a primary particle size of approximately 250 nm and a corresponding BET surface area of ~ 8.0 m^2/g.

Sr doped $LaMnO_3$

$La_xSr_{0.2}MnO_3$ ($0.7 \leq x \leq 0.79$) compositions were synthesized by the liquid mix technique using $La_2(CO_3)_3$, $SrCO_3$, and $MnCO_3$ as the raw materials. All raw materials were standardized thermogravimetrically to determine the cation concentration. The carbonates were dissolved in nitric acid, ethylene glycol, citric acid and water in glass beakers. Heating resulted in the formation of a polymeric precursor solution which was then oxidized at ~300°C. The powder was vibratory milled dry for 4 h with ZrO_2 media. The powder was then calcined in MgO crucibles at temperatures of 800 - 1200°C in increments of 100°C. Soak times for all calcinations was 4 h. The powders were vibratory milled again using the same conditions as described before. Powder

crystallinity, phase, and surface area were characterized using X-ray diffraction and BET techniques as a function of calcination temperature.

3.3 Single Cell Fabrication

The YSZ electrolyte used in this investigation was self supporting (~ 200 μm thick) and the cathode and anode were applied via screen printing onto a pre-sintered dense electrolyte. A flowchart describing the techniques used to fabricate single cells is shown in Figure 3.

Electrolyte fabrication

YSZ powders were initially dried at 150°C to remove any physically bonded water and then mixed with a commercially available binder system from Ferro Corp, B73210. This pre-mixed solution contains binder, plasticizer, solvents, and dispersants with a solids content of 18 wt%. The binder, and solvents are polyvinyl butyral, and ethanol and toluene, respectively. The dispersants and plasticizers in the binder system are proprietary. The proportion of YSZ to B73210 by weight was approximately 50/50. A glass release agent, M1111, and a surfactant, M1135, were added to the slip to facilitate removal of the dried tape from the glass and to improve the dispersion behavior of the YSZ powder, respectively. The glass release agent and surfactant were added at a ratio of 1 and 2 wt % of the total organic content, B73210. The slip was ball

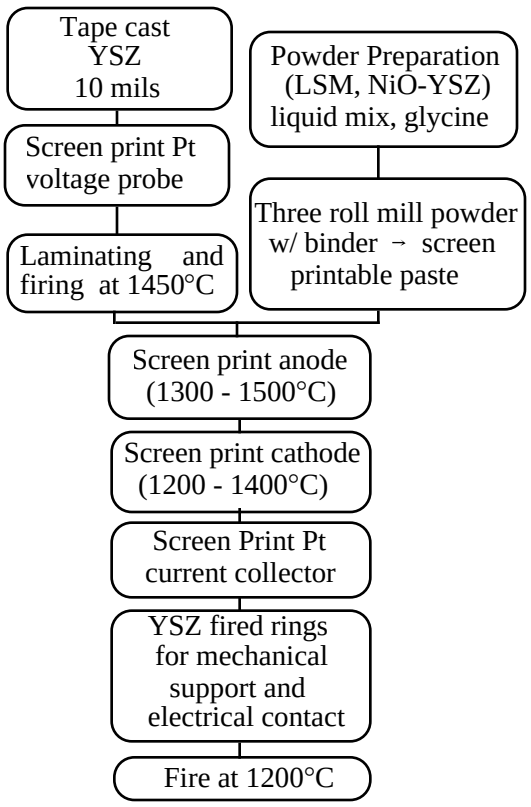

Figure 3. Flowchart of the techniques used for fabricating single cells

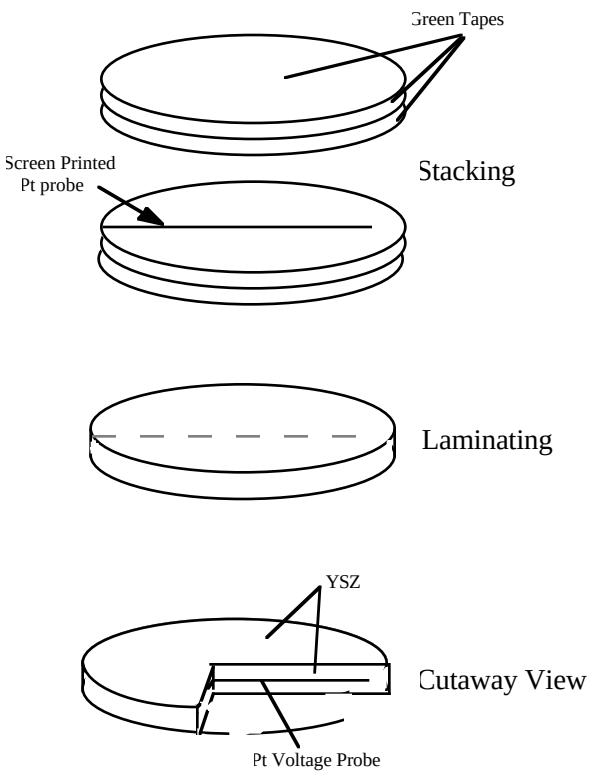

Figure 4. Stacking and laminating green YSZ tapes with a Pt probe in the center of the specimen.

milled with ZrO_2 media for 24 - 48 h until the powder was well dispersed. The rheological behavior of the YSZ slip was measured using a HAAKE Viscotester Model VT 500.

The slurry was tape cast using the doctor blade technique at a take-off height of ~250 μm and the resultant dried tapes were ~ 50-75 μm. Casting thickness can be varied by adjusting the doctor blade height but this value was chosen to help facilitate handling. The tape was dried for at least 24 h prior to use to ensure removal of all volatile species. The final proportion of powder to binder (total vol % solids in the tape) was approximately 50/50. Dried tapes were inspected with a light table to discard any defective regions. Circular samples of 2 inch diameter were cut out of the tape and a Pt voltage probe (38 mm long x 0.3 mm wide) was screen printed onto the YSZ tape. The Pt, E1170 (Ferro Corp.), is a fritless, screen-printable paste with a solids content of 70 wt %. A stainless steel 325 mesh screen with an emulsion thickness of 0.1 mil was used. The Pt probe was screen printed to the edge of the YSZ tape for electrical connection. The tape was again dried for at least 24 h prior to use to ensure removal of all volatile species from the Pt paste.

The tapes (six total) were stacked and laminated at 3000 psi for 10 min at 70°C in such a way as to place the Pt probe in the center of the fired specimen, Figure 4. The thermal processing schedule for binder removal and densification of the YSZ laminates was 0.5°C/min to 350°C, hold for 1 h, 3°C /min up to 1450°C, hold for 2 h, and then cool at 3°C/min. Sintered YSZ dimensions were 3.2 cm and 200 μm for the diameter and thickness, respectively. The sintered specimen underwent a shrinkage of ~25 % (x-y) during densification. The Pt voltage probe was centered internally 100 μm from either surface, and was ~ 5 μm thick and 200 μm wide.

Electrode deposition

The electrode powders were mixed with a commercial resin solution, BX018-16, from Ferro Corp. The suspension was mixed using a three roll mill to prepare a well-dispersed paste for screen printing. The wt% loading of powder to binder varied depending on the calcination temperature and resultant surface area of the powder and was therefore performed on a trial and error basis. In all instances the highest amount of powder was loaded into the binder such that the paste was still workable. For comparison, the LSM compositions calcined at 1200°C and 800°C had surface areas of 1 and 19 m^2/g and were thus loaded with 75 and 50 wt % powder, respectively.

The cathode compositions were screen printed onto dense YSZ electrolytes and sintered at various temperatures. Stainless steel screens of 230 mesh, 1 mil emulsion thickness were used. Cathode compositions were sintered onto the electrolyte between 1200°C and 1400°C in 100°C increments for a 1 h hold, with a heating and cooling rates of 3°C/min. A primary goal of this investigation was to vary the grain size and porosity of electrode microstructures and the their impact on electrode performance, therefore powders were calcined and sintered at various temperatures. Cathodes were porous, exhibited grain sizes on the order of 1μm, and gave resultant dimensions of 0.635cm x 0.635cm and ~ 20μm thick. Fracture surfaces were characterized by a JEOL Scanning Electron Microscope to examine resultant microstructures. All specimens were sputtered with Pd/Au before analysis.

Mechanical Support and Electrical Connection

A Pt grid (0.2 mm line width and 0.2 mm spacing between lines) was screen printed on the electrodes for cell performance experiments to act as a current collector but also to allow gas diffusion to the electrode/electrolyte interface.

Tape cast and fired YSZ rings (~ 350 μm thick) were bonded to both sides of the electrolyte using a ceramic adhesive, Aremco 516, Figure 5. The adhesive is a zirconia based cement which allowed thermal cycling without delamination of the rings from the electrolytes. The rings acted as both mechanical support for the electrolyte and for electrical connection. The mullite tubes used for atmosphere control were cemented to the rings rather than the electrolyte so that no adhesive was in the vicinity of the active region of the cell. The rings were designed with pads (half moon design) which were coated with Pt paste to allow for electrical sensing. Pt wires of 10 mil diameter were bonded from the Pt grid to the Pt pads on the rings using Pt paste, this was done to both the anode and cathode side of the electrolyte. Pt paste was also used to paint a conductive strip from the Pt voltage probe to a pad on the ring for voltage sensing. There are two pads on the cathode side, one for electrical connection to the cathode and one for sensing the voltage probe, whereas only one pad was active on the anode side. The cell was sintered at 1200°C for 1 h to densify the Pt and achieve a good bond between the YSZ rings and electrolyte.

Fabrication of Cathode Compositions for Conductivity Measurements

DC conductivity measurements were performed on electrode compositions to determine the resistive losses and their contribution to the total cell performance. The resistance was also used to determine if microstructures were changing as a function of time. Cathode compositions were screen printed on dense YSZ substrates and sintered at temperatures and conditions as described above. The dimensions of the electrodes are 0.635cm x 1.75cm and ~ 20μm thick. Four Pt electrodes were screen printed on the anode and cathode compositions and sintered on at 1100°C. The two inner electrodes were 0.635 cm apart and the distance between the inner and outer electrodes was 0.16 cm. Each Pt electrode was 0.16 cm thick.

3.4 Electrical Characterization

Electrical characterization of single cells utilizing the internal Pt voltage probe was investigated to simultaneously separate the losses attributed to each component (anode, electrolyte, cathode) and their interfaces (cathode/electrolyte and anode/electrolyte) during cell operation. The

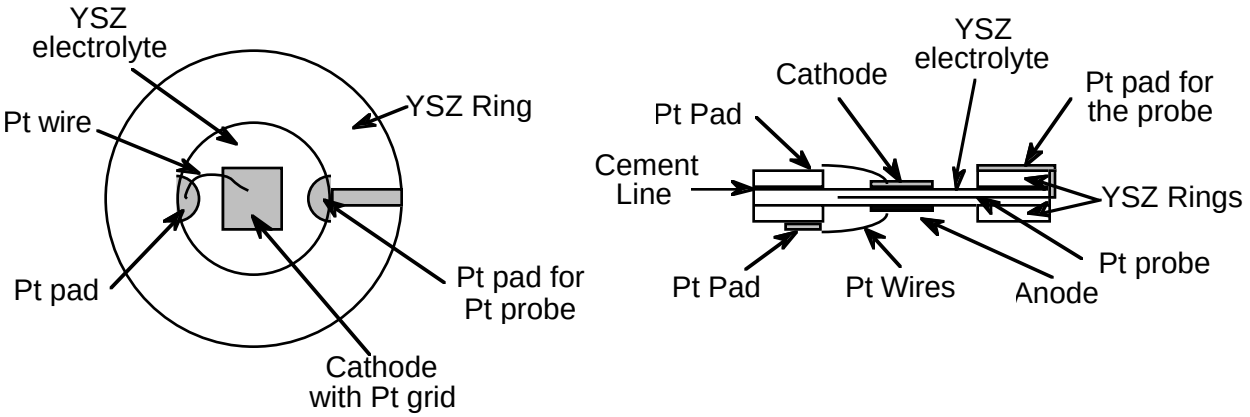

Figure 5. Addition of YSZ rings to the electrolyte for mechanical support and electrical contact.

cell performance studies were focused on the reaction kinetics at the interfaces whereas DC conductivity measurements were performed to investigate the resistive losses of each component as a function of time, composition, and preparation condition.

Cell Performance Studies

Electrochemical (I-V) measurements were carried out using a five electrode configuration which allowed for separation of anode and cathode overpotentials during operation, Figure 6. Separate leads were used to carry the current and voltage of the cell to remove the loss associated with the lead wires and allow for a direct examination of the losses attributed to the cell components. The third voltage lead was connected to the voltage probe and was used to monitor the voltage drop between the probe and corresponding electrodes during operation. Pt wires were used on the cathode side, four 20 mil wires for the current lead, and 10 mil wires for both the voltage leads, cathode and internal Pt probe. Ni wires were used on the anode side, two 20 mil wires for the current lead and a 10 mil wire for the voltage lead. Both voltage leads for the cathode and anode were designed to mimic a spring for contact with the Pt grids.

I-V behavior and AC impedance spectroscopy were performed on both half cells and complete cells. The I-V behavior was measured using an Anatronics Current/Voltage Control Fuel Cell Testing Module, a Keithley Model 196 Microvolt Meter, and a Fluke 27/FM Multimeter. The Fuel Cell Testing Module was placed in the voltage control mode thus enabling the desired cell voltage and corresponding current to be measured. AC impedance measurements were performed with a computer controlled Solartron 1260 Impedance/Gain-Phase Analyzer over the frequency range of 0.01 Hz to 100kHz with an applied signal of 20 mV.

After the cell was heated to 1000°C at ~ 2°C/min, air was first fed to the cathode and then the fuel was introduced to the anode. The fuel was delivered to the anode for at least thirty minutes before electrical contact was made to ensure that the anode (YSZ-NiO) was reduced to the cermet (YSZ-Ni). It could also be determined at this time if the electrolyte was cracked or the sealant had failed. The resistance between the voltage and current leads of each corresponding electrode was measured before testing to ensure that each lead was still connected to the Pt grid and thus the electrode.

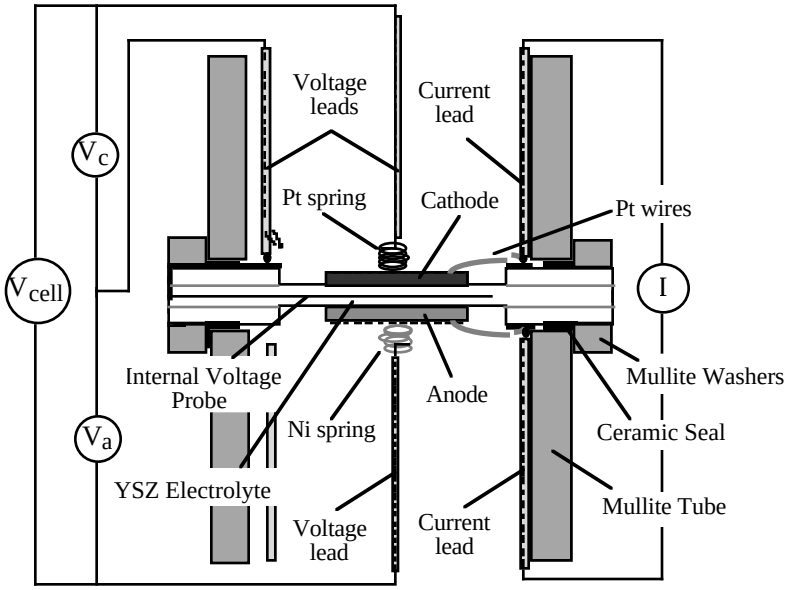

Figure 6. Experimental set up used for measuring the electrochemical (I-V) behavior of single cells.

After all electrical connections were made the first test was to measure the open circuit, Nernst potential between the anode and cathode. The Nernst potential is very sensitive to the chemical potential gradient and hence reveals whether a small hairline fracture had occurred. It was often difficult to tell this by monitoring the exit ball flow meters and were thus a better test for fractures or leaks.

Measurements were carried out from small voltages to larger ones in increments of 25mV and in all cases steady state voltages and currents were measured. Stabilization times were on the order of 2-3 min. The current, total cell voltage (V_{cell}), voltage drop from the Pt probe to the cathode (V_c) and the anode (V_a) were all simultaneously measured. At open circuit and at any given voltage under load the total cell voltage was equal to the two half cell voltages.

$$V_{cell}(I) = V_c(I) + V_a(I)$$

4.0 RESULTS AND DISCUSSION

4.1 Powder Characterization

This section examines the starting powder characteristics of commercial YSZ, and the synthesized Sr doped $LaMnO_3$ compositions. BET surface area and X-ray diffraction techniques were the principle methods used for characterizing the starting powders.

YSZ Powder

The commercial YSZ powder was characterized to confirm the supplier specifications, which stated the powder was fully stabilized (cubic) with a surface area and average particle size of $7.3 m^2/g$ and ~250 nm, respectively. X-ray diffraction was performed; the powder diffraction pattern has the cubic form, with no traces of the tetragonal or monoclinic phases. The BET surface area of the YSZ powder was measured to be $7.5 m^2/g$, which correlates well with the supplier's specifications. An average particle size was not measured, but was calculated using the following equation:

$$d = 6/(\rho \cdot SA)$$

where d is the average particle size (μm), ρ is the density (g/cm^3), and SA is the measured surface area (m^2/g). The calculated average particle size was ~140 nm and agrees with the reported values.

Sr doped $LaMnO_3$

$La_{0.79}Sr_{0.2}MnO_3$ compositions were calcined at temperatures between 800-1200°C, in increments of 100°C with 4 h dwells. The X-ray diffraction pattern for a $La_{0.79}Sr_{0.2}MnO_3$ composition calcined at 1100°C is shown in Figure 7. BET measurements were performed on powders calcined at temperatures ≥ 800°C, the results along with the calculated average particle size are shown in Table I.

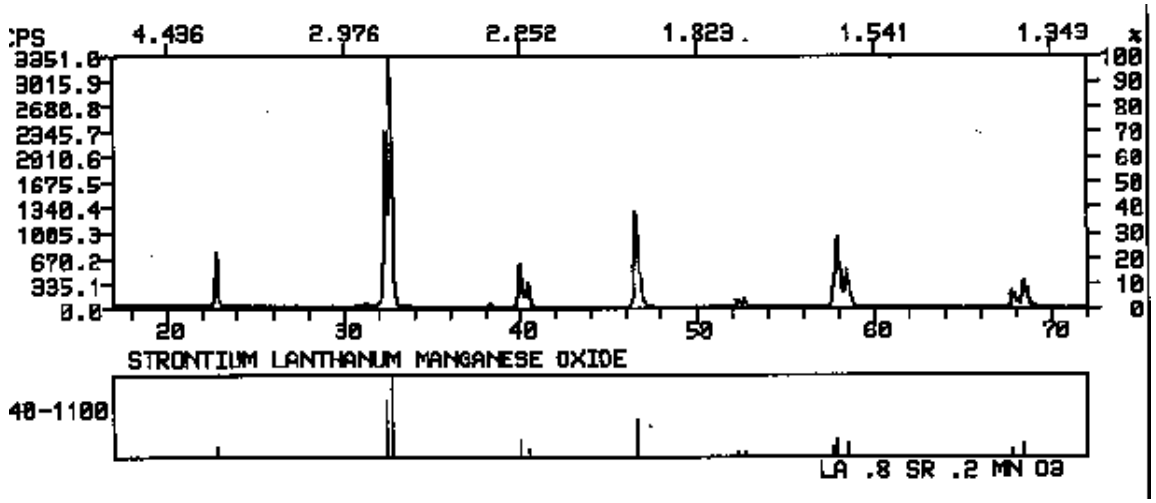

Figure 7. X-ray diffraction pattern for a $La_{0.79}Sr_{0.2}MnO_3$ composition calcined at 1100°C.

Table I.

BET surface areas, and calculated particle sizes as a function of calcination temperature for the $La_{0.79}Sr_{0.2}MnO_3$ composition.

Calcination Temperature (°C)	BET surface area (m^2/g)	Average particle size (μm) *
800	19.2	0.05
900	8.2	0.12
1000	3.4	0.3
1100	1.7	0.6
1200	0.9	1.0

* calculated by $d = 6/(\rho \cdot SA)$

Stoichiometric and nonstoichiometric compositions ($La_{0.79}Sr_{0.2}MnO_3$, $La_{0.75}Sr_{0.2}MnO_3$, and $La_{0.70}Sr_{0.2}MnO_3$) were analyzed using X-ray diffraction to determine if a second phase could be detected in the Mn excess compositions. A second phase was detected (Mn_3O_4) in the 10 % excess Mn composition calcined at 1200°C, the results are shown in Figure 8. The 100 % intensity peak for the Mn_3O_4 phase is at a 2θ value of ~36°, therefore, scans were made between 27 - 46°. The diffraction peak at ~38° is associated with the perovskite phase. A lower calcination temperature (900°C) was used for X-ray analysis to reduce the amount of Mn that could diffuse out of the sample by either the vapor phase or into the crucible during calcination. The 10 % excess Mn composition shows the Mn_3O_4 phase, whereas the 1 and 5 % excess Mn compositions do not show the presence of a second phase. For the case of the 5 % excess Mn composition, the amount of second phase present could be below the detection limit of the diffractometer.

4.2 Characterization of the Electrolyte

This section will examine the rheological behavior of the YSZ slip used for tape casting the electrolytes, density measurements on powder compacts as a function of temperature, electrical conductivity measurements, and some typical microstructures of the YSZ electrolyte with the buried Pt voltage probe.

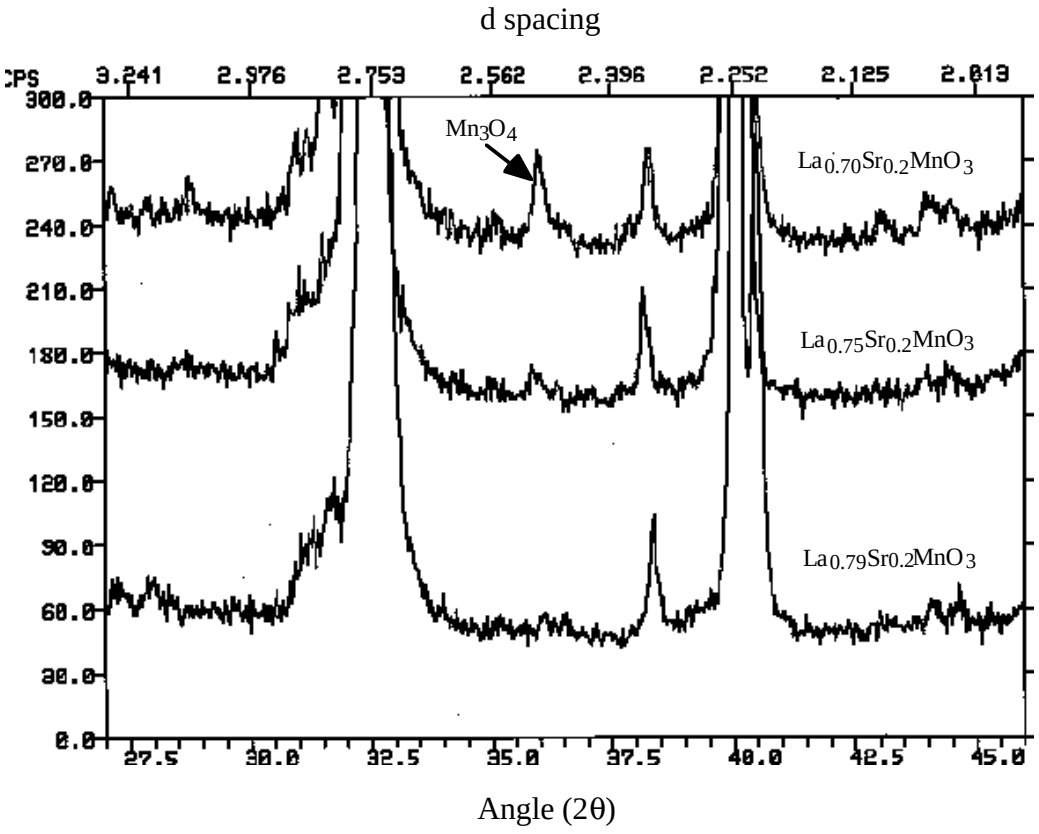

Figure 8. XRD patterns for the three $LaMnO_3$ compositions calcined at 900°C.

Rheological Behavior of the YSZ Slip

The rheological behavior of the YSZ slurry was determined by monitoring the viscosity as a function of shear rate, Figure 9. The behavior of the slip is pseudoplastic (shear thinning), the viscosity decreases with increasing shear rate. Pseudoplastic behavior is desired so that the slip flows during casting but displays little or no flow after casting, thus maintaining the desired cast shape.

Densification of YSZ Compacts

YSZ pellets were compacted and sintered in air between 1200-1600°C in increments of 100°C for 2h. Figure 10 shows the densification behavior of YSZ as a function of temperature. At 1200°C and 1300°C, densities of 85 and 96% of the theoretical were achieved. The theoretical density of YSZ is ~ 5.9 g/cm^3. Sintering temperatures of 1400 and 1500°C resulted in densities close to the theoretical (~99%). At higher temperatures, 1600°C, a decrease in density was observed, ~97% of the theoretical. A typical SEM micrograph of a thermally etched pellets sintered at 1400°C is shown in Figures 11. An increase in grain size was observed as the sintering temperature increased and a larger number of pores were present in the sample sintered at 1600°C, consistent with the density results. Samples sintered at 1400, 1500, and 1600°C resulted in grain sizes of ~ 5, 10, and 15 μm, respectively.

Electrical Conductivity of YSZ

The electrical conductivity of YSZ was determined by two different methods. The first method utilized sintered YSZ pellet, the resistance was measured as a function of temperature. Results of conductivity versus temperature for this method are plotted in Figure 12. The YSZ had a resultant conductivity of ~0.12 S/cm at 1000°C and an activation energy of ~1 eV. These values are consistent with those found in the literature. The second method employed two Pt probes buried in a YSZ electrolyte spaced 100 μm apart. The electrolyte with the two Pt probes

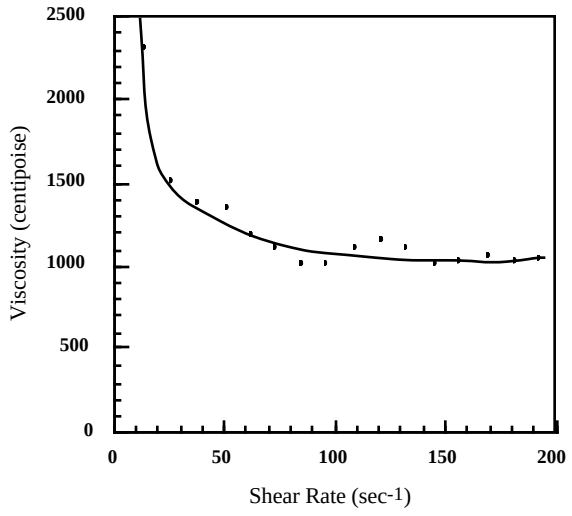

Figure 9. η versus shear rate of the YSZ slip used for tape casting.

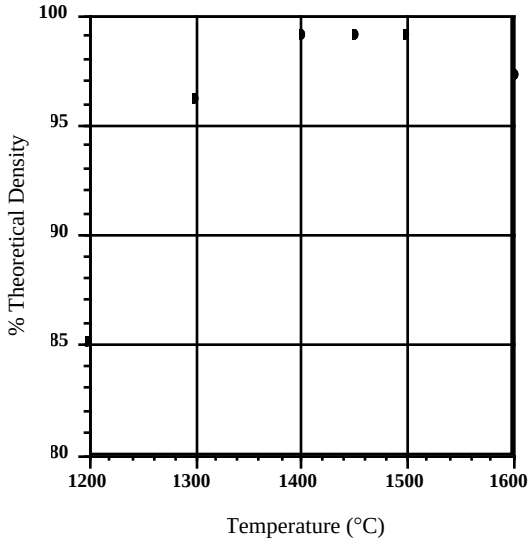

Figure 10. Density of YSZ compacts as a function of sintering temperature

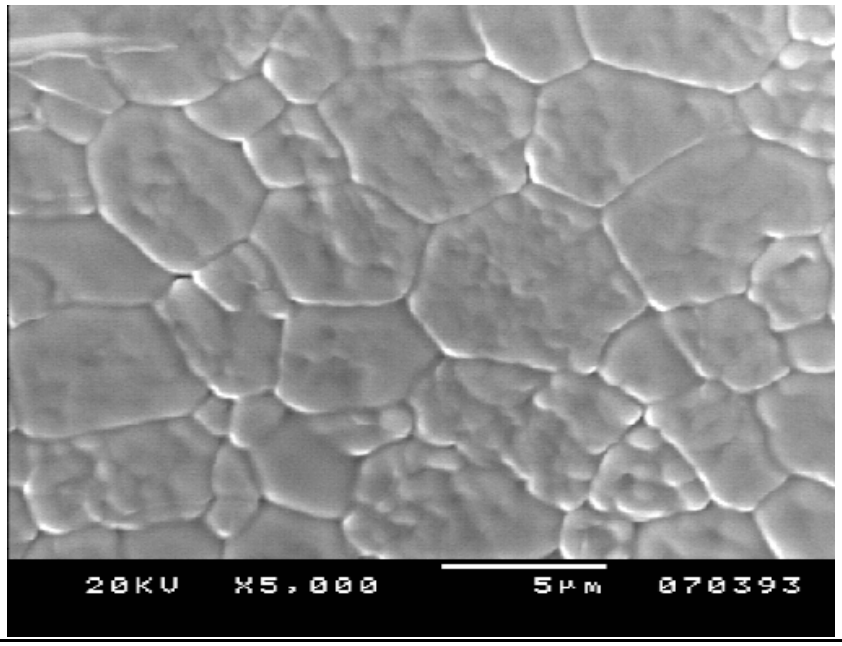

Figure 11. Thermally-etched YSZ sintered at 1400°C / 2 h.

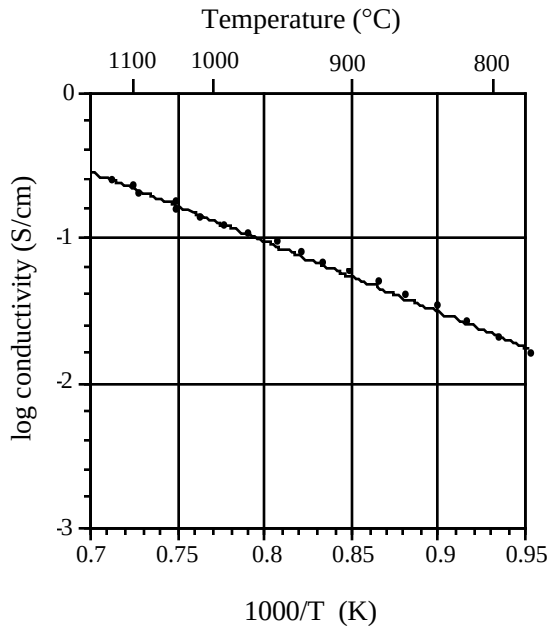

Figure 12. Log σ vs. 1/T for a YSZ compact in air.

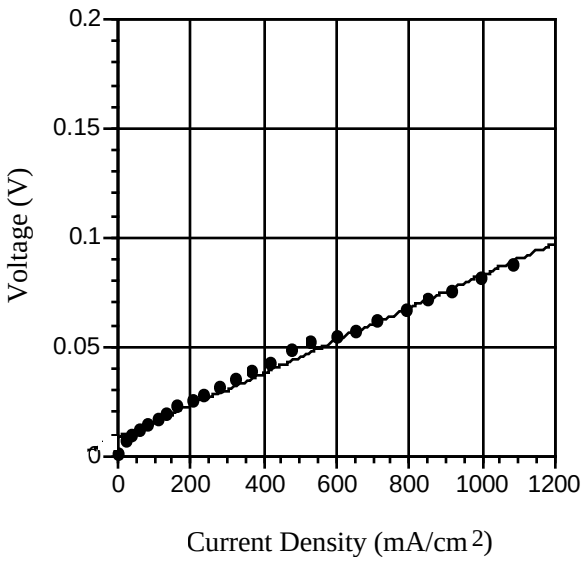

Figure 13. Voltage drop vs. current density of a 100 µm thick YSZ electrolyte at 1000°C.

was operated under fuel cell conditions at 1000°C. The voltage drop was monitored as a function of the current drawn through the cell, the results are plotted as voltage versus current density as shown in Figure 13. The voltage drop was ~82 mV at 1000 mA/cm^2 (400mA). The area of both the anode and cathode was 0.4 cm^2, and the resistance of the YSZ electrolyte was calculated to be

~0.21 Ω. The resultant resistivity and conductivity of the 100μm thick YSZ electrolyte was 8 Ω.cm and 0.12 S/cm, respectively. These values were consistent for those measured in the previous method.

The in-situ resistive loss measurements associated with the 100 μm thick electrolyte served as the basis for all cell measurements. A typical cell with a single Pt voltage probe buried into the center of the electrolyte (100 μm from the cathode and anode) is shown in Figure 14. The Pt probe is ~ 5 μm thick and 200 μm wide. Since all electrolytes had thicknesses of 200 μm and cathodes and anodes had electrode areas of 0.4 cm^2, the resistive loss associated with the electrolyte (82 mV at 1000 mA/cm^2) was used as a baseline for all cell experiment.

4.3 Experimental Determination of Electrode Overpotentials

In order to separate the cathode and anode overpotentials, the voltage was simultaneously measured from the Pt voltage probe to the corresponding electrodes. Cathode and anode overpotentials were calculated by subtracting the voltage drops under load from the corresponding voltage drops at open circuit:

$$\eta_{cathode}(I) = V_c@O.C. - V_c(I) - IR_{electrolyte} - IR_{cathode}$$

$$\eta_{anode}(I) = V_a@O.C. - V_a(I) - IR_{electrolyte} - IR_{anode}$$

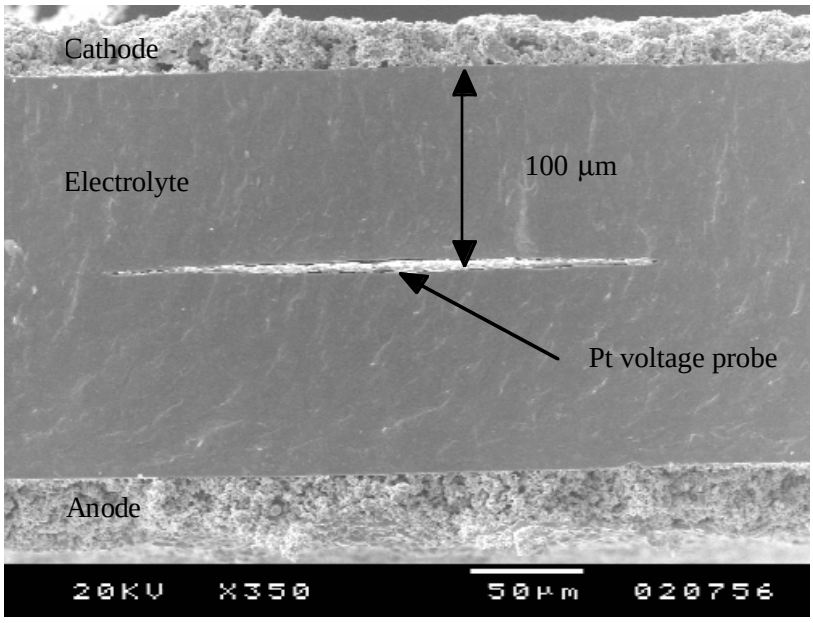

Figure 14. Typical cell with an internal Pt voltage probe.

where $\eta_{cathode}(I)$ = cathode overpotential
$\eta_{anode}(I)$ = anode overpotential
V_c@O.C. = voltage drop between cathode and Pt voltage probe at open circuit
V_a@O.C. = voltage drop between anode and Pt voltage probe at open circuit
$V_c(I)$ = voltage drop between cathode and Pt voltage probe under load
$V_a(I)$ = voltage drop between anode and Pt voltage probe under load
$IR_{electrolyte}$ = voltage drop associated with the electrolyte (100 μm thick)
$IR_{cathode}$ = voltage drop associated with the cathode
IR_{anode} = voltage drop associated with the anode

At open circuit and at any given voltage under load, the total cell voltage, V_{cell}, was equal to the two half-cell voltages

$$V_{cell}(I) = V_c(I) + V_a(I)$$

As described previously the resistive loss attributed to the electrolyte has been measured using two Pt probes spaced 100 μm apart within the electrolyte. For the cathode and anode overpotentials to be completely separated, the resistive losses from the cathode and anode were determined from 4-point DC conductivity measurements.

Total cell and electrode overpotential measurements were performed initially (~ 1-3 h under load) and after 24 h of operation. Initial experiments were performed at various times such that equilibrium current and voltage values were measured. After all electrical contacts were made and oxidant and fuel was delivered to the cell, the total cell voltage was decreased (maximum current condition). The voltage and current were both initially low but continued to increase with time (1-3 h) to a steady state value. The voltage was adjusted in increments of 25 mV and the current was monitored until open circuit values were achieved. By adjusting the cell to a low voltage (high current) condition, it was found experimentally to reach an equilibrium condition much faster than vice versa. After initial η-j experiments were performed, the total cell voltage was maintained at 0.7 V until the 24 h experiment was performed. The same was repeated for the 24 h measurement, experiments were started at low voltage (high current) conditions. The total cell voltage and the two half cell voltages were simultaneously monitored as a function of current.

3.4 Characterization of the Cathode

This section will describe the electrical characterization of the cathode directed at better understanding the effect of microstructure and composition on the resultant electrochemical behavior. Various characterization techniques were utilized to better understand resultant microstructures, and the separation of the resistive loss of the cathode from the electrochemical reaction at the cathode/electrolyte interface will also be described. All conductivity and cell experiments were performed at 1000°C in air with a flow rate of 200 sccm unless otherwise stated.

Resistive (IR) Contribution from the Cathode

Four point DC conductivity experiments were performed to determine the resistive loss attributed to the cathode. Cathode conductivities ranged from ~ 55 - 75 S/cm depending on the calcination and annealing temperatures (≥ 1200°C). Figure 15 is a typical V-I plot of a cathode demonstrating ohmic behavior.

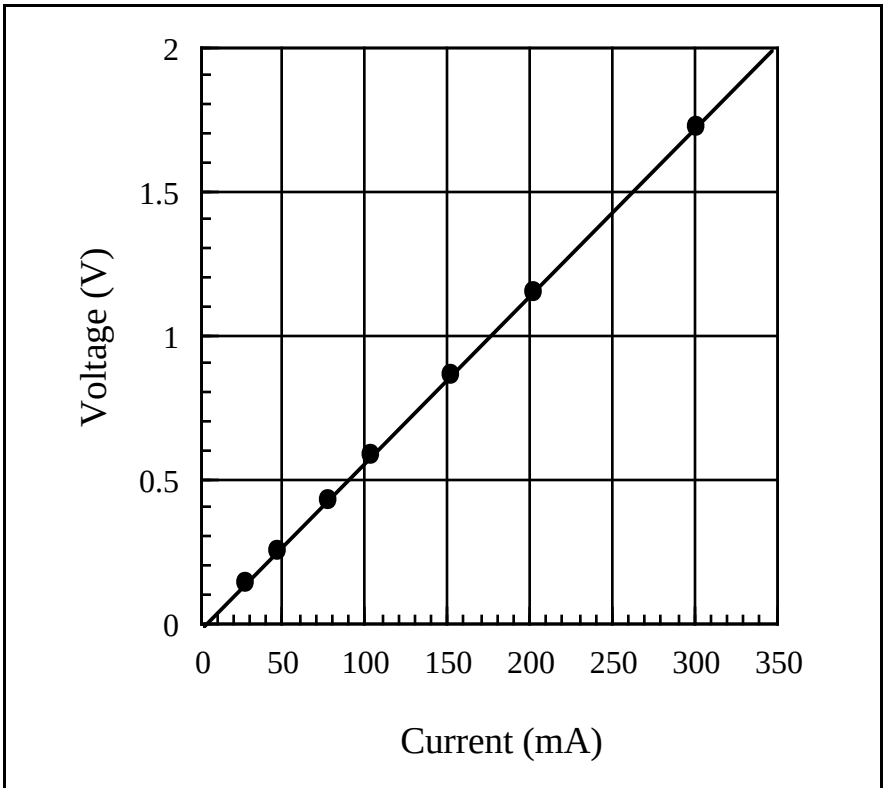

Figure 15. I-V behavior for a typical Sr-doped $LaMnO_3$ sample

The conductivities calculated in the four point DC conductivity measurements were used to calculate the resistance of the cathode in cell experiments. The cathode dimensions were the same for both types of experiments, but the current direction was different. The resistance was first measured and the conductivity was calculated in the plane, x-y, (area = 0.635 cm x 0.002 cm, thickness = 0.635 cm) for the four point DC conductivity experiment. The resistance was then calculated for the z-direction, (area = 0.635 cm x 0.635 cm, thickness = 0.002 cm) for cathodes in cell experiments. The lowest conductivity (55 S/cm) resulted in a resistance of 0.1 mΩ. This would correspond to a voltage drop of 0.04 mV at a current density of 1000 mA/cm^2. It will be shown in the following sections, plots of overpotential (V) vs current density (mA/cm^2), that the ohmic portion of the cathode is very small and cannot be resolved from the total measured voltage. Therefore, the measured voltage as a function of current density between the cathode and the Pt voltage probe can be attributed to the resistive loss with the electrolyte (100 μm thick) and the overpotential of the cathode.

Effect of Calcination Temperature of $La_{0.79}Sr_{0.2}MnO_3$ on the Electrode Reaction

$La_{0.79}Sr_{0.2}MnO_3$ (LSM) powders were calcined between 800 and 1200°C in increments of 100° for 4 h, prepared as pastes, screen printed onto YSZ electrolytes, and densified at 1200°C. The initial overpotential (η) - current density (j) results for these samples are shown in Figure 16. The resistive loss of the electrolyte (IR Electrolyte) has been separated and is also shown. All powders calcined below 1100°C show a similar electrochemical response with the 800 and 900°C calcinations showing the best performance (~ 60 and 80 mV at 1000 mA/cm^2). The lower calcination temperatures have a smaller particle size and would therefore be expected to contain more reaction sites (TPBs) for the oxygen reduction reaction to occur. The opposite would be true

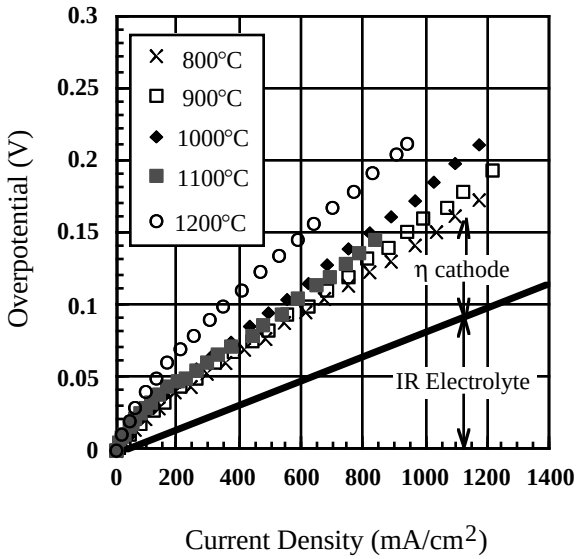

Figure 16. Initial η-j relations of the $La_{0.79}Sr_{0.2}MnO_3$ composition sintered on the electrolyte at 1200°C and calcined at various temperatures.

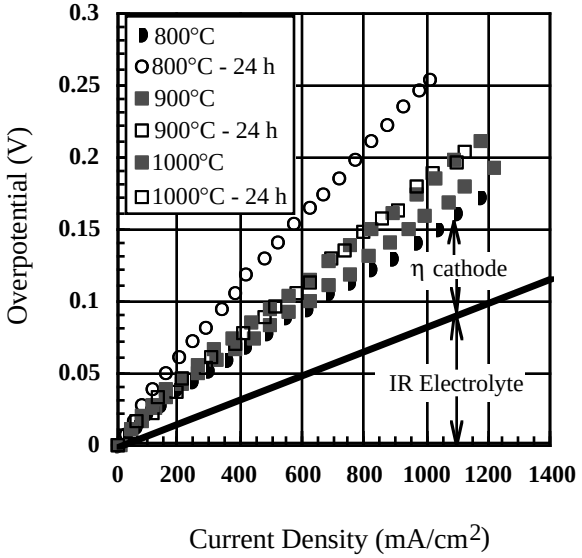

Figure 17. η-j relations initially and after 24 h of operation for the $La_{0.79}Sr_{0.2}MnO_3$ composition sintered at 1200°C and calcined at 800, 900, and 1000°C.

for the 1200°C calcination temperature. Although the samples are sintered onto the YSZ electrolyte at the same temperature, their still is the tendency for the lower calcination temperatures to initially have a smaller particle size (more TPBs). The sintering of the LSM onto the electrolyte is constrained even at 1200° due to the densified YSZ support, this is also enables porosity to be introduced into the cathode microstructure. All sintering occurs in the z-direction (into the plane of the electrolyte) rather than the x-y plane (in the electrolyte plane), there is no change in the area of the electrode before and after sintering.

Measurements were again performed on all samples after 24 h of operation. Powders calcined at 800 and 900°C were not stable with time and resulted in higher overpotentials. Powders calcined at temperatures ≥ 1000°C were stable within the 24 h time frame. Figure 17 illustrates the η - j behavior of samples calcined at 800, 900 and 1000°C as a function of time. The sample calcined at 800°C had the largest change in the overpotential and was comparable to the sample calcined at 1200°C (~ 170 mV at 1000 mA/cm^2). The 900°C sample also increased its overpotential but to a smaller extent (~ 100 mV at 1000 mA/cm^2). This can be explained by the powder further coarsening during operation which would give rise to a larger contact area and a reduced number of TPBs. The smallest particles are expected to have the highest driving force for densification which may explain the largest change in the electrochemical results for the 800°C calcination. Higher calcination temperatures (≥1000°C) may also show similar behavior for operation times greater than 24 h.

Figure 18 illustrates the microstructures after 24 h of operation for cathodes calcined at various temperatures and sintered at 1200°C. The SEM micrographs are fracture surfaces of the YSZ/LSM interface with the dense YSZ electrolyte at the bottom of each micrograph. The micrographs are better representations of the bulk electrode (grain size and pore size) than for determining the interfacial contact area between the YSZ and LSM, making analysis and interpretation difficult. The samples calcined at 1000, 1100, and 1200°C show consistent trends in their electrochemical behavior, higher calcination temperatures resulted in larger grain sizes and

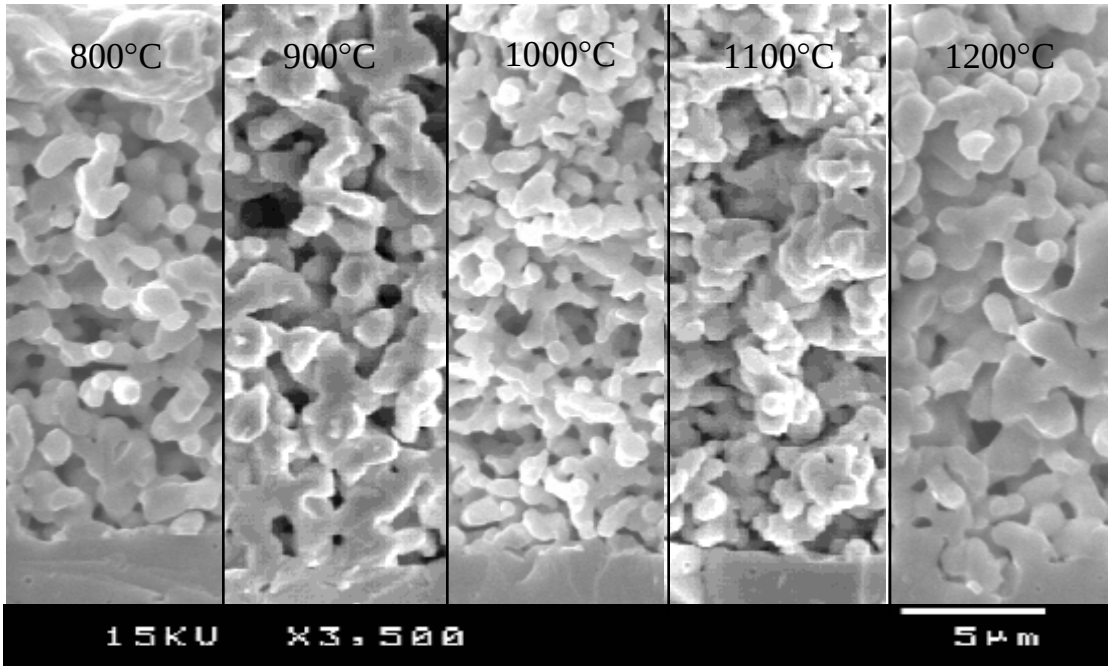

Figure 18. SEM micrographs of $La_{0.79}Sr_{0.20}MnO_3$ compositions calcined at various temperatures and densified onto the YSZ electrolyte at 1200°C.

higher overpotentials. The η-j results for samples calcined at 800 and 900°C suggests that the contact area and microstructure at the interface is changing with time. These microstructures are similar to the 1100 and 1200°C samples which is consistent with the electrochemical results. Other factors which could contribute to the overall cathode performance include: the density of the electrode, the pore size and pore size distribution, and the chemical interaction between LSM and YSZ. A second phase, $La_2Zr_2O_7$, was detected using X-ray diffraction at the interface between $La_{0.79}Sr_{0.2}MnO_3$ and YSZ sintered at 1200°C.

Effect of Composition and Sintering Temperature on Cathode Performance

The effect of nonstoichiometry (A site deficient or Mn excess) on Sr doped $LaMnO_3$ compositions was next performed using powders synthesized and calcined at similar conditions. The preparation conditions were the same in an attempt to suppress the effect of grain size, pore size, etc., but rather to gain a better understanding of the effect of excess Mn on the electrode reaction. This was first postulated using thermodynamic analysis to reduce the reaction product at the interface and thus lower the overpotential.

Powders Calcined at 900°C

The compositions studied were $La_{0.79}Sr_{0.2}MnO_3$ (1% excess Mn), $La_{0.75}Sr_{0.2}MnO_3$ (5% excess Mn), and $La_{0.70}Sr_{0.2}MnO_3$ (10% excess Mn) calcined at 900°C for 4 h then sintered on the YSZ electrolyte at temperatures between 1100-1400°C. The results will first be presented by comparing the three compositions fired on the electrolyte at similar temperatures, then the effect of the annealing temperature on each individual composition will be presented.

Figures 19-22 are η-j plots of the three compositions sintered onto the YSZ electrolyte at 1100, 1200, 1300, and 1400°C, respectively. The microstructures of the LSM compositions fired on the electrolyte between 1100-1400°C after 24 h of operation are shown in Figure 23. The microstructures for all three compositions were similar for each sintering temperature, therefore, only a typical microstructure after 24 h of operation for each annealing temperature representative of the three compositions is presented. The first overpotential plot, Figure 4.19, does not show any significant difference between compositions but does show an extremely high cathodic overpotential, ~300 mV at 1000 mA/cm^2. Due to the much finer microstructure of the LSM annealed at 1100°C (grain size ~ 0.5 μm) and greater vol % porosity, four point DC conductivity experiments were again performed to try to account for the large measured overpotentials. Initially, conductivity measurements were not performed on cathode sintered on the electrolyte at temperatures < 1200°C. The conductivity was calculated to be ~ 40 S/cm which gives a cell resistance of ~ 0.13 mΩ and a voltage drop of 0.05 mV at 1000 mA/cm^2. Therefore, this cannot account for the large measured potential drop between the cathode and Pt voltage probe. Adhesion of LSM compositions on YSZ is known to be poor for temperatures < 1150°C, which could be the main contribution in significantly increasing the measured overpotential. An electrode which has bad adhesion to the electrolyte would decrease the number of active sites for the oxygen reduction reaction for a given electrode area.

Figure 20 is the η-j plot of LSM compositions sintered at 1200°C. Only the results after 24 h of operation are presented, as is the case for the remainder of the results for the cathode overpotentials. For these compositions, especially the 5 and 10 % excess Mn compositions fired at higher temperatures (≥ 1200°C), the time to reach equilibrium became longer. These samples often improved (overpotential decreased) within the 24 h period. This has also been observed elsewhere, equilibrium was eventually achieved only after 100 h at lower operating temperatures (≤ 800°C). Data presented for the cathode overpotentials are the equilibrium values after 24 h of operation.

In Figure 20 a large variation is observed for the compositions, the 10 % excess Mn shows an extremely small overpotential (~ 40 mV at 1000 mA/cm^2). The 5% excess Mn composition also shows a lower overpotential (~ 80 mV at 1000 mA/cm^2) than the near stoichiometric sample (~ 105 mV at 1000 mA/cm^2). Because the grain sizes for the cathodes were observed to be very similar, this cannot be used as the basis for the large variation in the electrochemical behavior. X-ray diffraction was performed to see if a second phase (i.e. $La_2Zr_2O_7$) could be detected at the interface. Bilayer structures (LSM/YSZ) were fabricated in a similar manner as described for DC conductivity experiments with thinner cathodes (~ 7-8 μm). The cathode face was exposed to the X-ray beam to examine the LSM/YSZ interface. The XRD patterns for the three compositions annealed at 1200°C showed the same diffraction peaks corresponding to the YSZ and LSM phases except for the $La_{0.79}Sr_{0.2}MnO_3$ sample which had an extra peak at ~28.5°, corresponding to the 100 % intensity line of the $La_2Zr_2O_7$ phase. Therefore, the addition of excess Mn is effective in decreasing the pyrochlore phase formation at the interface at higher temperatures (≤ 1200°C). Quantitatively, nothing can be said about the pyrochlore phase except that the stoichiometric composition shows a greater amount of $La_2Zr_2O_7$ formed at the interface than the Mn excess compositions. The Mn excess compositions may also have the pyrochlore phase at the interface but may be small enough (i.e. thickness ~ Å or nm level) that it is not detected by the diffractometer. It would be predicted that the 5 % excess Mn composition should form the $La_2Zr_2O_7$ phase at the interface as a function of temperature and time before the 10 % composition. This would help explain the higher overpotentials. Another possible explanation for the difference in the electrochemical behavior for the 5 and 10% Mn excess sample (assuming no pyrochlore has formed at the interface) is that equilibrium has yet to be attained after 24 h.

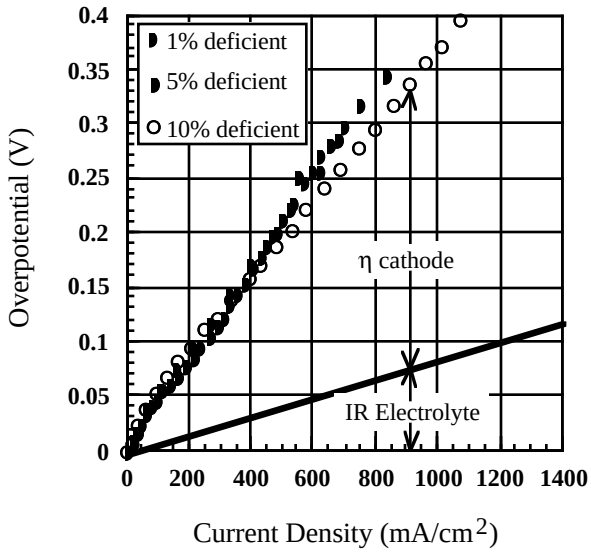

Figure 19. η-j relations of the three Sr doped $LaMnO_3$ compositions calcined at 900°C and sintered at 1100°C.

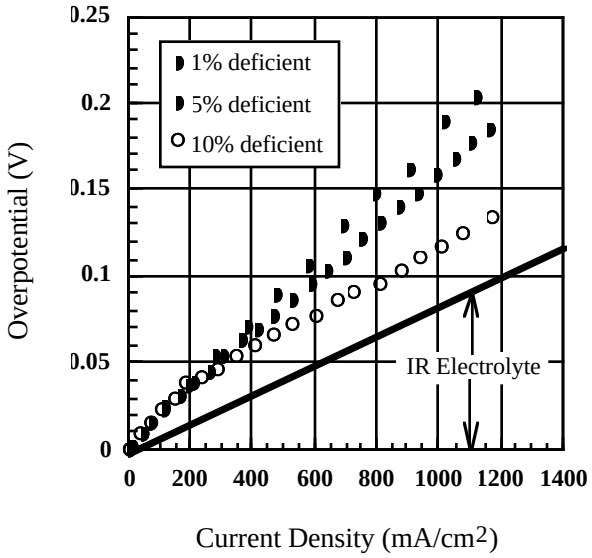

Figure 20. η-j relations of the three Sr doped $LaMnO_3$ compositions calcined at 900°C and sintered at 1200°C.

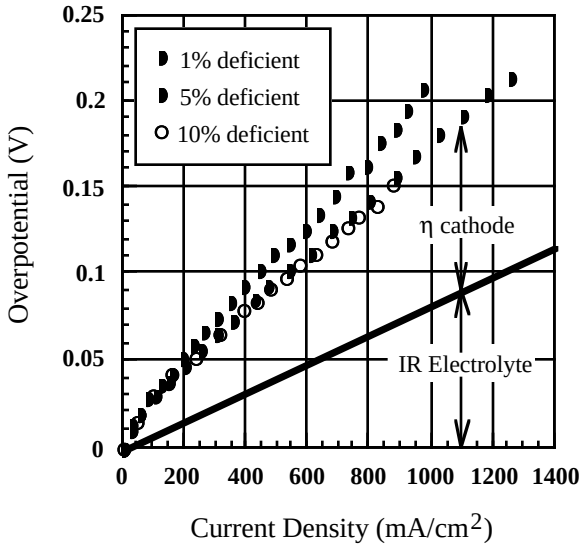

Figure 21. η-j relations of the three Sr doped $LaMnO_3$ compositions calcined at 900°C and sintered at 1300°C.

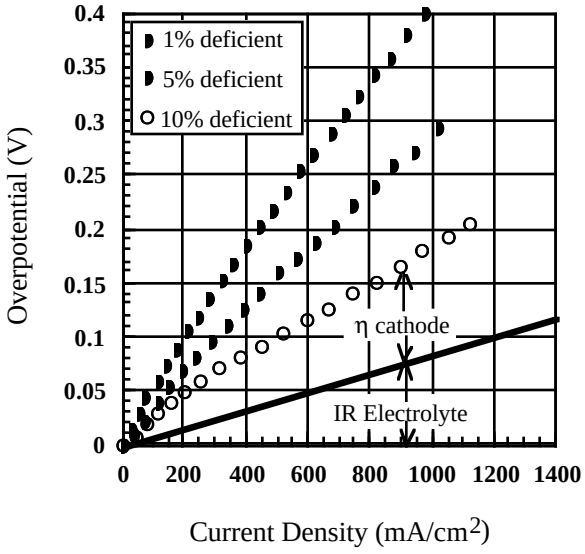

Figure 22. η-j relations of the three Sr doped $LaMnO_3$ compositions calcined at 900°C and sintered at 1400°C.

Figure 21 is the η-j plot of the three compositions fired at 1300°C. A similar type of trend is observed as was for the 1200°C firing except that the overpotentials have increased. The resultant overpotentials for $La_{0.70}Sr_{0.2}MnO_3$, $La_{0.75}Sr_{0.2}MnO_3$, and $La_{0.79}Sr_{0.2}MnO_3$, at 1000 mA/cm^2 are ~ 90, 100, and 130 mV. The increase in the measured overpotentials compared to the lower sintering temperature (1200°C) can be attributed to both an increase in the grain size (less TPBs) and a greater amount of $La_2Zr_2O_7$ formed at the interface. It is assumed that more Mn would diffuse into the YSZ, resulting in a thicker interfacial reaction product, as the temperature and time of exposure were increased.

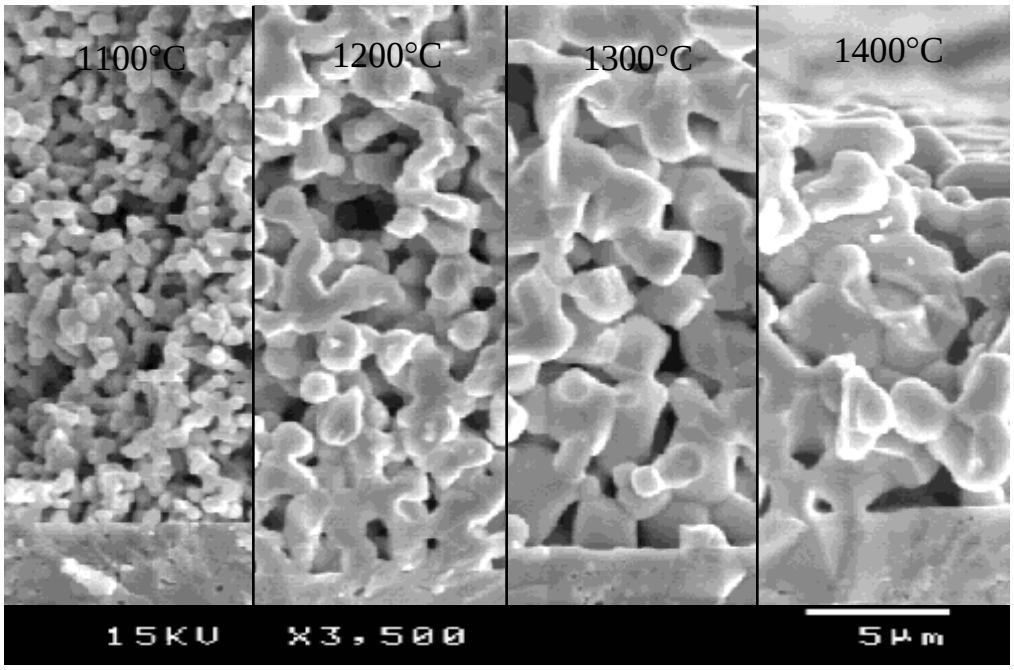

Figure 23. Microstructures of typical Sr doped $LaMnO_3$ compositions calcined and sintered on the YSZ electrolyte at various temperatures. calcined at 900°C and sintered at 1200°C.

The overpotential results for the three compositions fired at 1400°C are shown in Figure 22. The 1 % and 10 % excess Mn compositions show a consistent trend with the lower sintering temperatures, namely, that the overpotentials are larger due to both a larger grain size and an increased reaction at the interface. The overpotential values for the 1 and 10 % excess samples at 1000 mA/cm^2 are ~ 210 and 100 mV. The 5 % excess sample has a very high overpotential (~ 320 mV at 1000mA/cm^2), and is not consistent with the previously observed trends. Some possible explanations could be that the sample was cracked or improperly sealed which allowed the mixing of the fuel and oxidant which could reduce the oxygen pressure in the cathode chamber. Another possible explanation is that the sample has not equilibrated within the 24 h period.

The three compositions were also sintered onto a YSZ substrate at 1450°C to see if a second phase could be detected using the SEM. The resultant microstructures of the YSZ/LSM interfaces are shown in Figure 24. No second phase at the interface was observed, therefore, X-ray diffraction was used to analyze the bilayers as described previously. All three composition show the pyrochlore phase development at the interface. Again, nothing quantitative will be said about the amount of $La_2Zr_20_7$ formed at the interface.

The Effect of Flow Rate and Gas Composition

The flow rate of the oxidant (air) used in all previous experiments was maintained at 200 sccm. Air was delivered at 100, 200, and 300 sccm to observe the effect of flow rate on the cathodic overpotential. The cathode used for this experiment was a $La_{0.70}Sr_{0.2}MnO_3$ composition calcined at 1200°C and sintered on the YSZ electrolyte at 1200°C. The cell was allowed to equilibrate at 1000°C for 24 h before measurements were performed. The results for various flow rates are shown in Figure 25. There is a slight difference between the 100 and 200 sccm flow rates

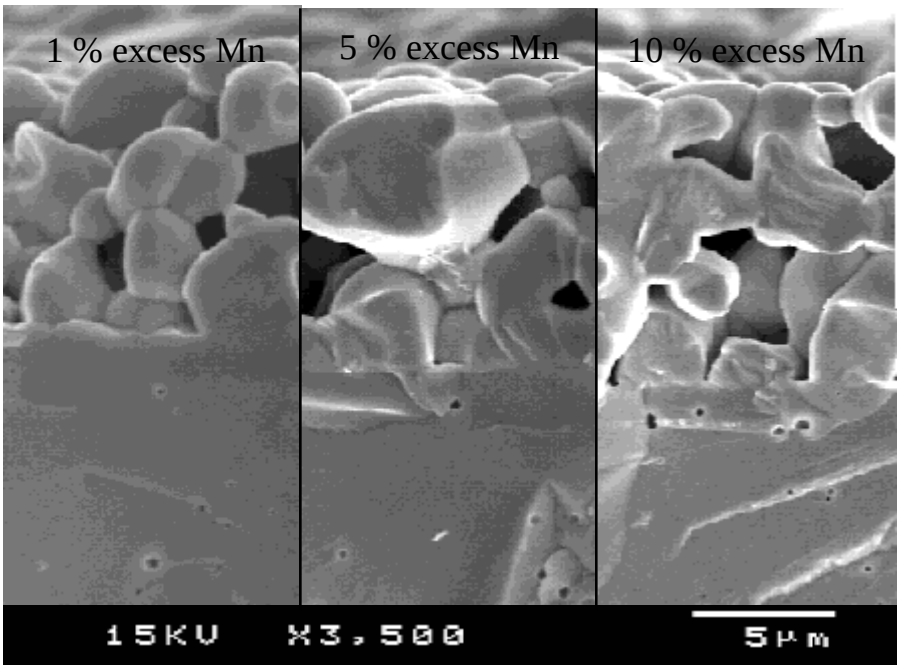

Figure 24. Microstructures of $La_{0.79}Sr_{0.20}MnO_3$, $La_{0.75}Sr_{0.20}MnO_3$, and $La_{0.70}Sr_{0.20}MnO_3$ sintered on the YSZ electrolyte at 1450 °C for 24 h.

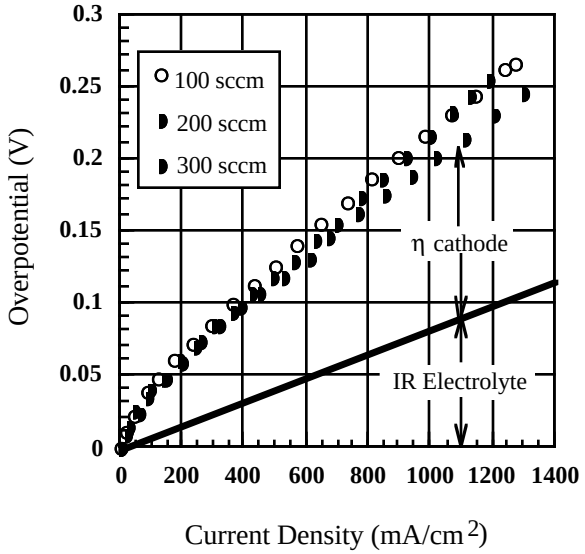

Figure 25. η-j relations as a function of flow rate for a Sr doped $LaMnO_3$.

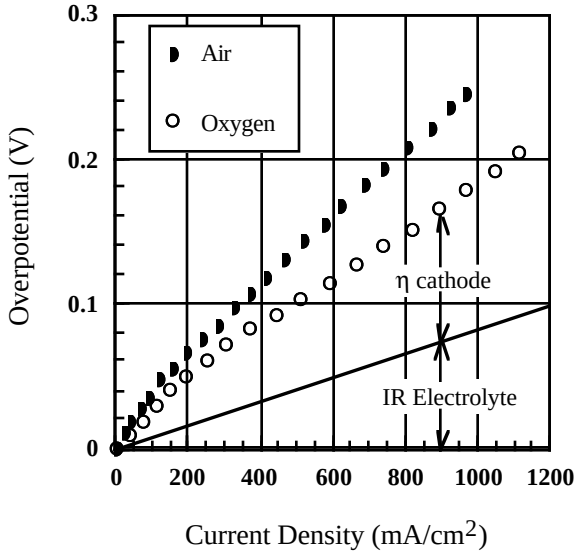

Figure 26. η-j relations for a Sr doped $LaMnO_3$ with air and oxygen used as the oxidant.

(both are ~ 135 mV at 1000 mA/cm^2), but the higher flow rate of 300 sccm did show a decrease in the overpotential (~ 120 mV at 1000 mA/cm^2). The decrease in the overpotential was attributed to a greater supply of oxygen to the cathode.

Since a higher flow rate of air decreased the cathodic overpotential, the effect of pure O_2 compared to air was next examined. Both O_2 and air were supplied to the cathode at the same flow rate, 200 sccm, and the results are shown in Figure 26. The overpotential for pure O_2 (~ 100 mV at 1000 mA/cm^2) showed a significant decrease compared to air (~ 170 mV at 1000 mV/cm^2). The open circuit voltages were comparable to the theoretical values for pure O_2 and air. The increase in the overpotential is believed to be due to the difficulty in removing the N_2 within the electrode, this is known as "flooding". The N_2 would thus block some of the active sites for oxygen reduction and result in an increased overpotential. The use of air over oxygen is therefore giving rise to a diffusional overpotential at the cathode.

5.0 MAJOR ACHIEVEMENTS DURING THE PAST YEAR

Cathode Studies:

- Increasing the particle size of the $La_{1-x}Sr_xMnO_3$ cathode results in higher overpotentials, but lends long term stability at 1000°C. Increasing the cathode firing temperature increases the overpotential, although the microstructure remains fairly constant. Although 800°C yields the best initial results, after 24 h of operation the overpotential climbs sharply. We have found that 1000°C gives the best performance/stability combination. At 1 A/cm^2, the cathodic overpotential is ≈0.1 V, which is very good

- Nonstoichiometric $La_xSr_{0.20}MnO_3$(x=0.70, 0.75, and 0.79) cathode compositions exhibit the best properties. Previously-summarized results showed that A-site deficient compositions exhibited the lowest overpotentials. To further explore this effect, we completed a series of studies using these compositions fired on at temperatures of 1100, 1200, 1300 and 1400°C. In all instances, 1200°C was the optimum, with the x=0.70 composition being the best. It has an overpotential of only 0.04V at 1 A/cm^2. SEM analyses indicated no second phases or interdiffusion is detectable. Longer time studies are underway.

Electrolyte Studies:

In addition to initiating studies on thicker electrolytes, we have developed a new technique of measuring the overpotentials which occur at the cathode and anode. In this technique a Pt voltage probe is buried directly in the electrolyte by tape casting and screen printing techniques. We have successfully used this structure to directly measure the spatial variation of the overpotential. By placing electrodes at different positions within the electrolyte we can measure the potential at both the cathode and anode under different cell driving conditions. Results have been published: D. M. Reed, H.U. Anderson, and W. Huebner, "Characterization of Solid Oxide Fuel Cells by Use of an Internal Pt Voltage Probe," *J. Electrochemical Soc.*, **143**[5] 1558-1561 (1996).

6.0 FUTURE ACTIVITIES

With respect to the major thrusts of this program:

- Fabricate single cells with controlled microstructures of the anode; incorporate interfacial modifications to improve the catalytic activity.

- Gain a better understanding of the mechanisms involved in improving cell performance via electrochemical and impedance techniques.

7.0 ACKNOWLEDGMENTS

We gratefully acknowledge the technical interactions with our METC COR, William C. Smith. The period of performance for this program is 4/16/93 through 4/15/98.